Emissivity correction using spectrum correlation of infrared and visible images

Yunlai Gao[1,3], Gui Yun Tian[2,3*]

1. College of Automation Engineering, Nanjing University of Aeronautics and Astronautics, Nanjing 211106, China
2. School of Automation Engineering, University of Electronic Science and Technology of China, Chengdu 611731, China
3. School of Engineering, Newcastle University, Newcastle upon Tyne, NE1 7RU, UK

Abstract

Thermography is a typical sensing approach used for non-destructive testing and evaluation (NDT&E). However, the varying surface emissivity of an object leads to illusory temperature inhomogeneity which results in influences on defect detection. This paper proposes a new technique to correct the influence of the surface's varying emissivity of an object in active thermography. Two cameras operating at different spectra are used to capture infrared and visible images simultaneously. Although the physics behind infrared and optical imaging are very different, a close spectrum correlation of two images is identified. An invariant coefficient feature has been estimated for an emissivity correction of infrared images with suggested algorithm. The basic hypothesis is that the reflectance correlation is proposed to predict surface emissivity of an object with respect to wavelength. Experimental validation results show that after correction infrared images are looking like more homogeneous and independent of emissivity. It has been tested for a partially painted steel and rail samples with different known emissivity. Comparative analysis demonstrates its promising capability for accurate mapping of thermal patterns and defect evaluation in thermography NDT&E.

Keywords: thermography NDT&E; emissivity correction; spectrum correlation; two cameras measurement

1. Introduction

Infrared thermography has been widely used for non-destructive testing and evaluation (NDT&E), which allows inline visualization of thermal patterns to identify defects and material degradations [1-3]. It is effective for material variation monitoring by capturing thermal contrast between defective and non-defective areas of test objects [2-4]. It has the advantages of non-contact temperature measure, wide spectrum response, high resolution imaging over a large area etc., which is suitable for automatic scanning inspection and moving target thermal imaging in real-time [5-8]. However, one of the disadvantages of thermography is that the infrared radiation strongly dependent on surface emissivity of an object [9-11]. All targets above -273.15°C (0 K) emit radiant energy, where an ideal emitter or blackbody is defined as a 100% emitter of energy. The ratio between the actual energy emitted from a real object and that of a blackbody emitter is known as emissivity and always $\leqslant 1$. The emissivity is mainly dependent on object surface conditions [9-12], e.g. shiny or roughness, material composition, wavelength. In thermography NDT&E, the varying emissivity in local positions influences the accurate mapping of thermal patterns. It leads to illusory temperature inhomogeneity of infrared images which results in influences on defect detection and characterization [12-15].

To reduce surface emissivity influence, various methods have been attempted in previous studies [13-16]. The black paint on sample is effective to raise emissivity for uniform distribution. However, this method easily leads to the pollution of sample and it is infeasible for online scanning application. To eliminate the emissivity factor from the thermal radiation equation, Bai et al. [13] proposed the normalization method to remove emissivity adverse influence of eddy current pulsed thermography (ECPT) and improve thermal contrast between defective and defect-free regions. In Kasemann's study [16], relative emissivity distribution was employed to correct temperature errors based on a ratio of emissivity with the average value. Vellvehi et al. [17] conducted irradiance-based emissivity

correction to determine true temperature based on two reference thermal images obtained at two uniform temperatures. Schubert et al. [18] corrected emissivity changes in rough or textured surface based on mathematical deconvolution. The phase information is also used to reduce or to enlarge surface emissivity variation influences [14, 19-20]. Gao et al. [21] proposed a thermal pattern separation model to remove emissivity influence. Schmugge et al. [22] implemented temperature and emissivity separation from multispectral thermal infrared observation using relative emissivity values.

Additionally, spectral emissivity estimation using single, dual and multiple wavelength approach is available to measure temperature accurately [23-25]. The utilization of multi-spectrum information is potential to reduce surface emissivity influence [24, 26]. Firstly, optical pyrometers (also known as brightness pyrometers) measure temperature in the visible light spectrum of 0.4 to 0.7 µm [23]. Next, infrared thermometers measure temperature in the infrared light spectrum of 0.7 to 80 µm. Both optical and infrared temperature measurement are influenced by emissivity. But, the emissivity can be addressed based on the center wavelength of the spectral band being utilized [24, 27]. By combining infrared and visible imaging information e.g. reflectance in different spectral windows, the normalized difference vegetation index (NDVI) [28, 29] was used for emissivity correction in remote sensing. Hagqvist et al. [25] used historical emissivity and temperature information for estimating the current emissivity, which is named emissivity compensated spectral pyrometry. Tachikawa et al. [30] combines the thermography and visible imaging to separate the influence of emissivity and temperature.

This paper proposes a new technique to correct the influence of the surface's emissivity of an object in active thermography. The infrared and visible light cameras operating at different spectra are used to capture two modality images simultaneously. Based on the optical properties of metals and the physics behind infrared and optical imaging [31-33], a close spectrum correlation of two modality images is identified. An invariant coefficient feature is suggested for an emissivity correction of infrared images. Experimental studies have been implemented on the optimized ECPT system and two partially painted samples with different known emissivity. The validation and comparative results demonstrate the promising capability of the method for accurate mapping of thermal patterns and further defects characterization under natural environments. The rest of this paper is organized as follows. Section 2 introduces theoretical background and the proposed method for emissivity influence correction. Section 3 demonstrates experimental studies using the optimized ECPT system with two modality cameras. Section 4 implements results and comparative analysis based on two samples with different known emissivity. Conclusions and future works are derived in Section 5.

2. Theory and Proposed Method

Based on the physical principles of infrared and optical imaging [26, 31], a close spectrum correlation of infrared and visible images is identified. The method using two cameras measurement is proposed for an emissivity correction of infrared images. The images pre-processing including automatic registration, segmentation and the algorithms with calculation of correction coefficient [34, 35] are implemented. It is used to reduce the varying emissivity influence on the accurate mapping of thermal patterns for defect evaluation.

2.1 Physical basis of infrared radiation and thermography

Thermography allows a direct measure of the emitted infrared radiation energy, then temperature distribution of an object is determined in a non-contact way by using infrared camera. According to the Stefan-Boltzmann law [13], the radiation energy from an object can be expressed as:

$$j^{\star} = \varepsilon \sigma T^4 \qquad (1)$$

where the irradiance $j^{\star}$ is energy radiated per unit time per unit area. It is directly proportional to the fourth power of the black body's temperature T. The Stefan-Boltzmann constant σ derives from other known constant of nature $\sigma = 5.67 \times 10^{-8} Wm^{-2}K^{-4}$. An actual object emits less total energy than a black body and is characterized by an emissivity ε $(0 < \varepsilon < 1)$. The emissivity of an object is given by the ratio between energy emitted by a blackbody

and actual object having same temperature. It presents a material's ability to emit thermal radiation and is an optical property of matter [11, 12]. To understand the nature of emissivity for real object at steady-state, infrared energy exhibits the properties of absorption, reflection and transmission to varying degrees [30, 33]. The opaque object e.g. metal exhibits very low transmission of infrared energy, hence, there is a simple balance between emissivity and reflectivity which can be expressed as:

$$\varepsilon + \rho = 1 \qquad (2)$$

where ρ denotes as surface reflectance of an object. Based on the equation (2), reflectance is proposed to predict spectral emissivity of an object in a specific range of spectrum. Additionally, the emissive and reflective behaviors of materials have some correlation in both visible and infrared spectra [30, 31]. The metal object with shiny surface condition demonstrates lower emissivity and higher reflectance. Hence, reflectance ρ can be used as a proxy for 1- ε, which paves a way to quantify the emissivity character and surface conditions of an object [24]. As described in [23-25], one essential requirement for multi-wavelength pyrometry is obviously the choice of an adequate emissivity model for normalization [36]. Because no universal model exists, various models for different range of spectrum e.g. MWIR and optical spectra that could possibly be adapted to various specific cases should be studied. This paper proposes two cameras measurement to obtain infrared and visible images simultaneously. As two cameras operate at different spectra, the thermal emissivity and optical reflectance cannot meet the equation (2) directly in the corresponding pixels. The basic hypothesis is that the surface emissivity in the infrared and the reflectivity in the visible light behavior should be a refined correlated way e.g. using different weights. Algorithms and coefficient feature are suggested to compute the weights and to perform an emissivity correction of the infrared images.

2.2 Spectrum correlation of infrared and visible images for emissivity correction

To achieve an emissivity correction of infrared images, two cameras are used to capture both infrared and visible images simultaneously. The visible image provides brightness information to identify surface spectral reflectance, color and surface roughness of an object. The thermal image gives us the total infrared radiation coming from object surface, which includes reflection and emission. Although two cameras operate at different spectra with different physics, there are some close correlations between visible and infrared images response to a same object, e.g. higher reflectance and lower emissivity in shiny conditions [30]. Based on the physical characters of infrared and visible imaging, the paper uses the brightness of an optical image as a proxy for reflectance ρ and identify the relationship to infrared image. The procedure and weighting functions with coefficient feature are proposed for an emissivity correction of infrared images as illustrated in Fig. 1. The input information from the visible and infrared images should be obtained independent on any surrounding environment influences. A uniform incident light source and special shielding arrangements can be used to avoid the ambient undesired lighting and the reflection effect due to external thermal radiation. The de-noising, scaling and rotation of two images are carried out in pre-processing for automatic registration. When presenting the setup, it is recommended that the spatial compensation between pixels and angular of the modality images are corresponded as the work [37]. The image segmentation is carried out to identify spectrum correlation of infrared and visible images in different local areas. The algorithms and invariant coefficient calculation for emissivity correction of infrared images is carried out by two steps below with respect to wavelength. The validation of the proposed method is implemented and discussed by experiments and comparative analysis with previous methods [4, 13].

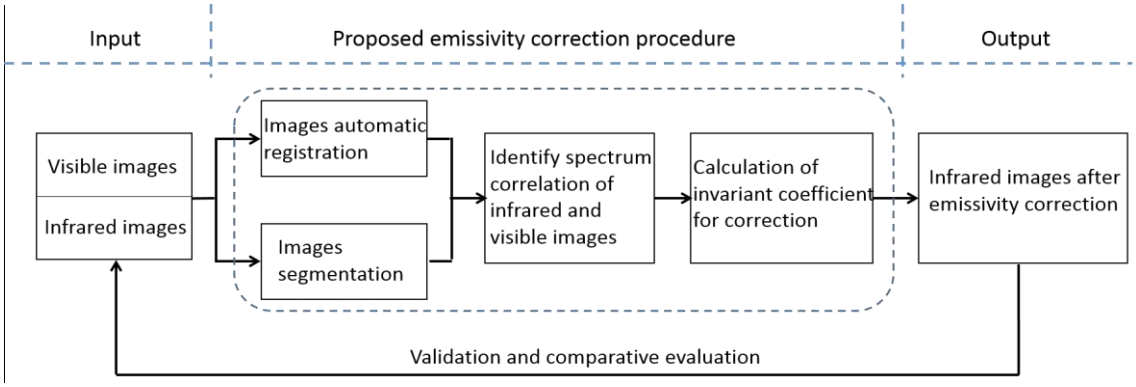

Fig. 1 Diagram of emissivity correction using spectrum correlation of infrared and visible images

Step 1: To compensate infrared and visible imaging scales using *k* weight.

For the two cameras operate at different spectra, the pixel value of infrared image $I_T(\varepsilon, T)$ depends on surface emissivity ε and temperature T of an object according to equation (1), and the brightness of visible image $I_V(\rho, I_{cd})$ indicates surface reflectance ρ of an object and incident light source intensity I_{cd}. With a same temperature on the surface of an object, infrared image $I_T(\varepsilon)$ is only related to the emissivity of each pixel point with respect to a specific wavelength. It also can be written as $\varepsilon(I_T)$ under a specific temperature T. By using a uniform incident light source, visible image values $I_V(\rho)$ demonstrate surface reflectance distribution of an object, which is defined as reflected light intensity by a surface, divided by that received by that surface. It also can be written as $\rho(I_V)$ under a specific incident light intensity I_{cd}. Hence, combine the $\varepsilon(I_T)$ and $\rho(I_V)$ based on the equation (2) with proper weights, it can be rewritten to the equation (3) where the infrared and visible images are added together and equal to a constant. It is in the conditions that there is a specific roughness on the surface of an object and without any influences of the surrounding temperature and lighting of ambient environment. The suitable calibration of two cameras is required for spatial compensation between pixels and angular of images [37]. The integration of infrared and visible images is applied with different scale factors k including surface emissivity, lighting condition, camera characters including gain balance as well as surface characteristics in line with equation (2). Of course, the k weight is varied with different locations considering surface temperature distribution of an object and incident light source intensity.

$$k \times I_T + (1 - k) \times I_V = \text{constant} \quad (3)$$

where the I_T denotes as the pixel value of the infrared image with a specific temperature, and the I_V is the brightness value of the visible image with a specific incident light source intensity. According to the equation (3), the linear relationship between infrared and visible images against emissivity is illustrated in Fig. 2. The pixel value of an object thermal image is ranging from I_{T0} to I_{T1} with different emissivity ε. The brightness value of visible image is ranging from I_{V0} to I_{V1} with different reflectance ρ or 1- ε. In consideration of equation (3), the infrared and visible values variation against different emissivity, e.g. from shiny to black body behaviors, are changing to the opposite trend. Considering the slopes of the infrared and visible values variation in Fig.2, the k weight can be calculated based on the derivation of the equation (3) to emissivity ε, which is defined as $k = (-\Delta I_V)/(\Delta I_T - \Delta I_V)$.

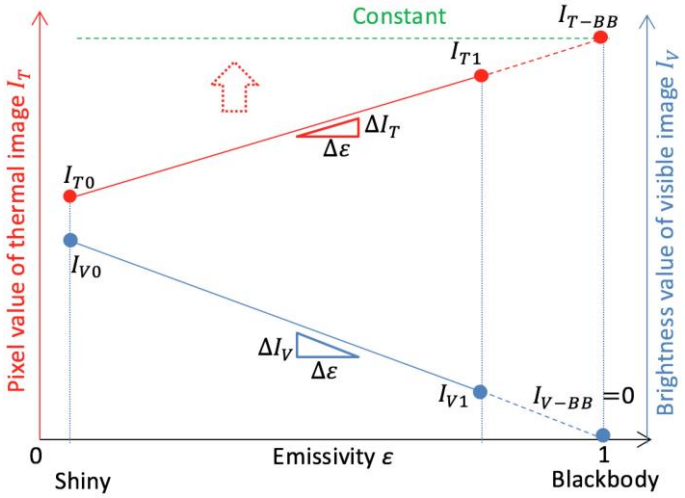

Fig. 2 Linear relationship between infrared and visible values against emissivity

Step2: To correct emissivity influence through infrared image to 'black body' image

In order to reduce emissivity influence on the mapping of thermal patterns, the aim is to make the infrared image behaving more homogeneous with a specific temperature and looking like to a same or uniform emissivity behavior in each pixel point. Hence, a specific condition that infrared value of the blackbody I_{T-BB} is selected to define the "constant" in equation (3). With the ideal situation of blackbody behavior, the brightness value of visible image I_{V-BB} is equal to zero because the reflectance of ideal blackbody is zero. The algorithm for emissivity correction is to make the different pixel values of thermal image are independent on the emissivity and close to the "constant" value I_{T-BB}, which is like a blackbody object behaves to a specific temperature.

To implement an emissivity correction of infrared images, an invariant coefficient feature $\Delta I_T/\Delta I_V$ is extracted through the equation (4). This equation is obtained from Fig. 2 considering the slopes of infrared and visible values response to different emissivity. Because the $\Delta I_T/\Delta\varepsilon$ and $\Delta I_V/\Delta\varepsilon$ are based on the physical spectrum responses to surface emissivity and reflectance of an object [30, 31], the invariant coefficient feature $\Delta I_T/\Delta I_V$ is independent of the contents e.g. unknown emissivity of imaging results in different local areas. Then, the emissivity influence is reduced and corrected according to the equation (5) with coefficient feature and an extra correction factor α. The α is an additional correction factor considering actual object and surrounding environmental influences in real applications [8, 32]. It makes infrared image more homogeneous under a specific temperature and independent of emissivity, which is close to the one behaving like blackbody with uniform emissivity distribution. The corrected infrared images including accurate mapping of thermal patterns are used for further defect detection based on thermography NDT&E. Experimental studies using two partially painted samples including slot-like artificial cracks and natural cracks are conducted for validation and comparative evaluation.

$$\text{Invariant coefficient} = \frac{\Delta I_T/\Delta\varepsilon}{\Delta I_V/\Delta\varepsilon} = \frac{\Delta I_T}{\Delta I_V} = 1 - 1/k \tag{4}$$

$$\text{Corrected IR image} = I_T + \frac{\Delta I_T}{\Delta I_V} \times I_V + \alpha = I_T + (1 - 1/k) \times I_V + \alpha \tag{5}$$

3. Experimental studies and validation

To validate the proposed method for an emissivity correction of infrared images, experimental studies have been performed on a steel plate and rail samples with different known surface emissivity. The diagram of the optimized ECPT system using both infrared and visible cameras is illustrated in Fig. 3. Two images on the surface of a same object are captured and recorded by two cameras simultaneously for processing.

3.1 Optimized ECPT system with two modality cameras

The optimized ECPT system is based on our previous developed ECPT system, which combines both advantages of pulsed eddy current [38, 39] and thermography. The system includes a pulse generator, the Easyheat 224 induction heater and water cooling devices, excitation coil, an infrared camera and a PC as described in references [3, 40-41]. The difference is here we use two cameras to capture both infrared and visible images simultaneously as illustrated in Fig. 3. For experimental studies, the electric current with amplitude of 380 A_{rms} and frequency of 256 kHz is applied on the coil to stimulate heat on the surface of an object for a period of 200ms. The FLIR A655sc infrared camera with uncooled microbolometer detector and spectral range 7.5-14 μm is used to record surface thermal radiation of test object. A selected resolution with 640×240 array and the frame rate 100 Hz of the IR camera are applied to capture transient infrared images within the duration of 2 seconds. The infrared camera has been calibrated by the FLIR Company using blackbody calibration source. An optical camera with 1280×960 array is used to record the visible image and brightness on the top surface of test object simultaneously. Two cameras are placed at the same position and calibrated to same view angle for capturing infrared and visible images at the same time. The spatial compensation between pixels and angular is made by two cameras calibration and two images registration as the work [37]. A PC is used for images processing and emissivity correction using the proposed method. To avoid the surrounding environment influences, the ambient undesired lighting and the effect of reflection of external thermal radiation are reduced by special shielding arrangements.

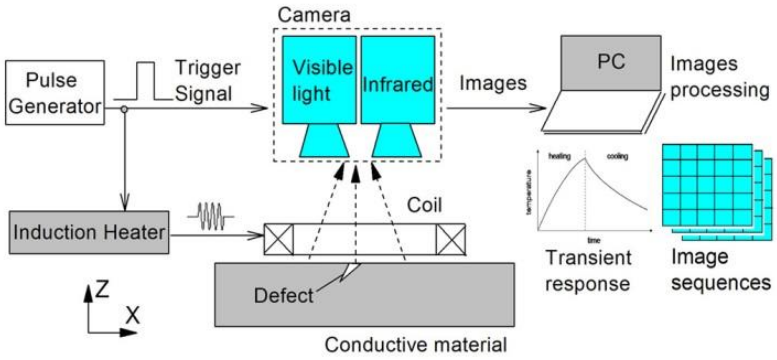

Fig. 3 Diagram of the optimized ECPT system with both infrared and visible cameras

3.2 Sample preparation with different known emissivity

Two samples with different known emissivity are employed for experimental studies as shown in Fig. 4. A steel plate includes a slot as well as local shiny and black painting areas as shown in Fig. 4a. The known shiny and black painting indicate two different emissivity regions on the surface of the plate. According to the references [10, 17], the emissivity of the black painting and steel shiny surface are close to 0.96 and 0.07, respectively, under mid wavelength IR windows (MWIR) with spectral band $8-14\ \mu m$. The size of steel plate is $11.5\text{mm} \times 17.5\text{mm} \times 1\text{mm}$ in width, length and thickness, respectively. The heating coil with 6.35mm wire diameter is placed at the back of sample for heating and thermography in transmission mode. It is also placed at the middle position of a slot with $15\text{mm} \times 0.5\text{mm}$ in length and width to compare the thermal patterns around the defect. As shown in Fig. 4b and 4c, the second sample is a rail head piece including rolling contact fatigue (RCF) multiple cracks. The emissivity on the rail sample is known with different shiny, sparse and normal black painting as shown in Fig. 4c, then applied full uniform painting in Fig. 4b for comparison. The heating coil is fixed on the top of the rail sample across different emissivity areas with 0.5mm lift-off distance. In real applications, image segmentation is implemented along with coil direction in order to obtain correction weights and invariant coefficient in different local areas considering temperature distribution and incident light intensity. To use the proposed method with unknown emissivity, the maximum and minimum values of infrared image under a specific temperature or a calibrated sample with known emissivity can be used as a reference for emissivity correction.

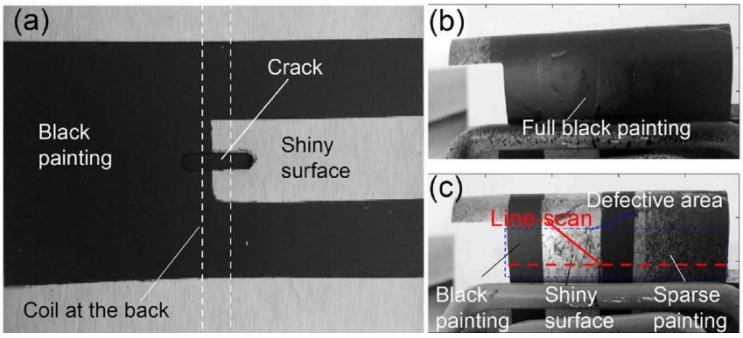

Fig. 4 Samples with different known emissivity, (a) steel plate including a slot with local shiny and black painting, (b) rail head sample with full uniform black painting and (c) local different painting where the defective area includes natural multiple cracks

4. Results analysis and discussion

To correct the emissivity influence on infrared images and defect detection, experiments on two samples with different known emissivity have been carried out to capture infrared and visible images simultaneously. As the two images are captured by two different types of cameras operating at different spectra, the scaling, rotation, segmentation and automatic registration of two images have been conducted in pre-processing for images pixel-to-pixel corresponding. A close spectrum correlation between infrared and visible images is verified considering surface emissivity and reflectance behavior of the test objects. The validation of the proposed method is discussed with comparing results.

4.1 Spectrum correlation analysis of infrared and visible images

To identify the emissivity and reflectance responses, Fig. 5 illustrates several line-scanned values of infrared and visible images. The images are captured from different known emissivity regions on the rail sample. The line-scanning direction is parallel to the heating coil with a specific distance as shown in Fig. 4c. The infrared value is the pixel value of the thermal image at the end of the heating time. The visible value is the brightness or gray value of the visible image. The sum of the infrared and visible value is based on the described method in section 2.2. In order to do comparison and avoid the different amplitude scale influence of the two images, the normalized amplitude is calculated based on all of the pixel point values of the individual image. A low-pass filter is applied on the line-scanned signals to avoid surface roughness influences.

According to the two line-scanned values on different surface conditions of the sample from Fig. 4c, it can be identified that the infrared and visible values present opposite amplitude responses to shiny and black painting areas. The line-scanned infrared values of the sample from Fig. 4b are similar along with the coil in different line-scanned positions. It means the infrared values demonstrate similar behavior to the similar temperature and emissivity by full black painting. The line-scanned infrared values from Fig. 4c present the radiation or emissivity responses higher to black painting and lower to shiny surface. On the other hand, the line-scanned brightness values of the visible image present higher reflectance to shiny surface and lower one to black painting regions. The opposite variation trend of infrared and visible values verified the spectrum correlation and the linear relationship of two images response to different emissivity conditions from the shiny, sparse painting to full black painting as shown in Fig. 5. Through the sum of infrared and visible values with the specific weight factor, the proposed method gives the feasibility to correct the influence of surface's emissivity of an object in infrared thermography. It demonstrates the promising results not only reduce the emissivity variation influence but also improve the measurement sensitivity of infrared values in shiny area.

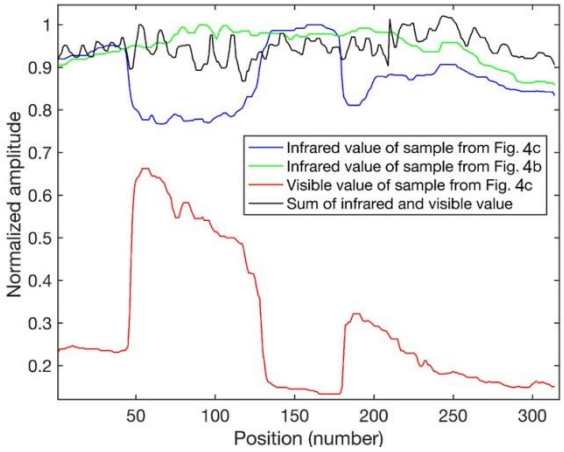

Fig. 5 Line-scanned values of infrared and visible images along the coil with different known emissivity on the rail sample from figure 4b and 4c.

4.2 Validation of emissivity correction method on different samples

The spectrum correlation of infrared and visible response with the monotonic relationship is used to validate the proposed method for emissivity correction. According to the line-scanned results in Fig. 5, the sum of infrared visible values is based on the equations (3-5), which means the infrared values in different emissivity regions are all corrected close to a "constant" value independent of the emissivity and be like infrared values response to black painting area. Extending the line-scanned result to full image processing, the emissivity correction of infrared images is implemented by experiments and the calculation of various correction coefficients considering different emissivity regions. Experimental results including infrared image patterns, spatial and transient responses before and after correction have been analyzed with different known emissivity on a steel plate and rail samples.

4.2.1 Validation on steel plate with two emissivity regions

The emissivity correction results of the steel plate by using two images is illustrated in Fig. 6 for validation. The shiny and black painting surface conditions represent two different known emissivity regions. As shown in Fig. 6a, the infrared image before correction shows different mapping of thermal patterns in two emissivity regions. The infrared values in the black painting area are higher than them in the shiny region. In contrast to Fig. 6a, the brightness value of the visible image indicates the opposite response to surface conditions of the sample as shown in Fig. 6b. The infrared image after emissivity correction provides accurate mapping of thermal patterns around the heating coil and slot, which is continuously changed between shiny and painting areas along with the coil direction. Compared to previous methods using the normalization and phase features in references [13, 14], the proposed method provides real infrared values or temperature for accurate mapping of thermal patterns and defect characterization as shown in Fig. 6c. However, it should be noted that the infrared image in Fig. 6c needs more improvement by the optimization of algorithm with extra correction factors to reduce surrounding environment influences etc. [8, 32].

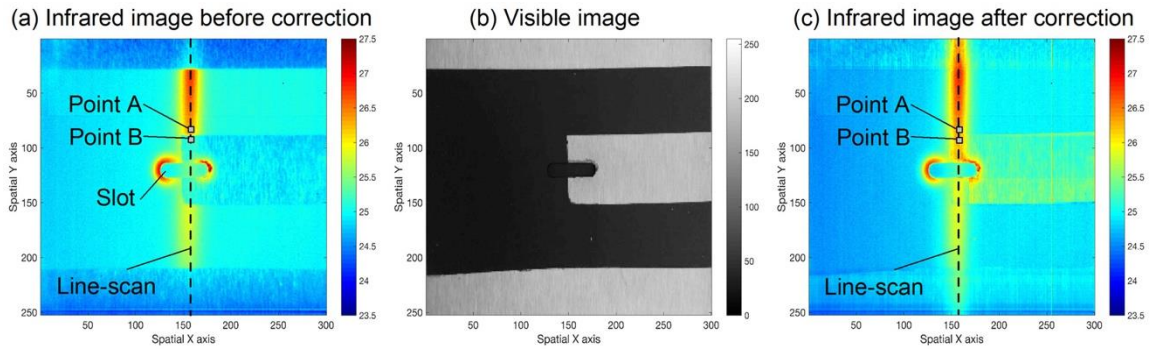

Fig. 6 Emissivity correction of the steel plate sample through the combination of two modality images, (a) infrared image at the end of heating, (b) visible image and (c) infrared image after emissivity correction.

The differences of spatial and transient infrared values with different emissivity between black painting and shiny areas are used to evaluate the performance of the proposed method and estimate the error for emissivity correction. The Fig. 7 illustrates infrared values from the line-scan and selected two points A and B as shown in Fig. 6c. As shown in Fig. 7a, the line-scanned low infrared value in shiny areas is amplified similar to the big value in paint regions. It is easier to identify the defect information based on the higher thermal contrast around the slot as shown in the green dotted circle area in Fig. 7a. The continuous variations of line-scanned values after correction demonstrate the correct thermal response in different positions, which is independent on the surface emissivity of the sample. The Fig. 7b shows that infrared values of the point B are corrected and enhanced close to the point A value during the whole heating and cooling times. Comparing the point B values before and after correction, the measurement sensitivity of the infrared value in the shiny condition is improved. Because the points A and B are neighbor to each other along the coil direction, they should have same temperature responses regardless of the black paint and shiny surface conditions. Based on the Fig. 7b, the mean square error (MSE) of the point B to the point A is calculated between the original and recovered infrared images. The MSE value before correction with 0.84 and after correction with 0.0059 give the objective assessment of the method for emissivity correction of infrared images. The results in Fig. 6 and Fig. 7 demonstrate the promising capability of the proposed method for emissivity correction and accurate mapping of thermal patterns for defect characterization.

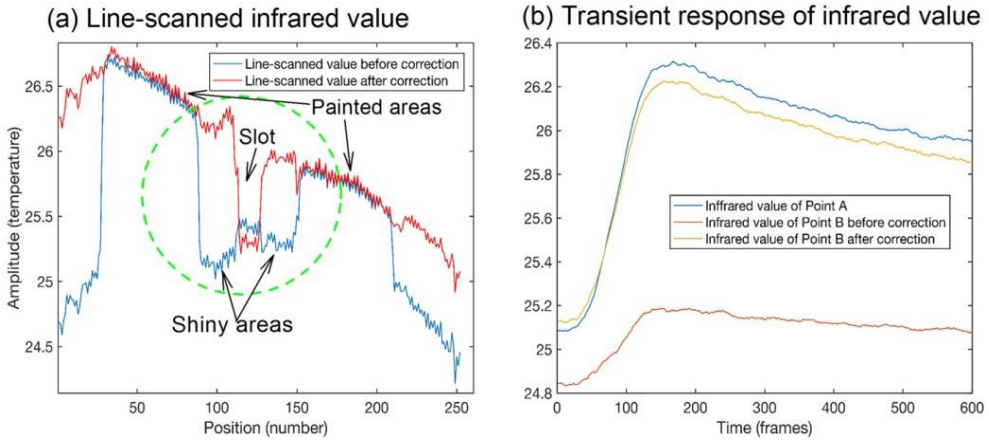

Fig. 7 Infrared images values comparison before and after emissivity correction, (a) specific line-scan infrared value and (b) transient thermal response with selected two points A and B from figure 6.

4.2.2 Validation on rail sample with complex emissivity distribution and natural cracks

The proposed method is expected to reduce emissivity influence and improve defect detectability of ECPT technique for rail inspection. The infrared and visible images of a rail sample from Fig. 3c with complex emissivity distribution and natural cracks are illustrated in Fig. 8 for the validation. It can be seen that the cracks in the black

painted area are clearly indicated by thermal patterns and contrast as shown in Fig. 8a. However, there is no distinct thermal contrast in the shiny region for crack characterization because of the emissivity influence. The visible image presents higher reflectance in the shiny area than black painted one as shown in Fig. 8b. After emissivity correction, Fig. 8c presents the recovered thermal patterns to indicate all of the natural cracks information without the influence of the sample surface conditions and emissivity. The infrared values in the shiny area are enlarged with higher thermal contrast for crack evaluation. The proposed method by using two images provides the accurate mapping of thermal patterns, which is independent of the complex surface emissivity. It improves the performance of the ECPT technique for natural crack characterization [4] with better measurement sensitivity of infrared values and higher thermal contrast between defective and non-defective areas in the shiny surface conditions of the sample.

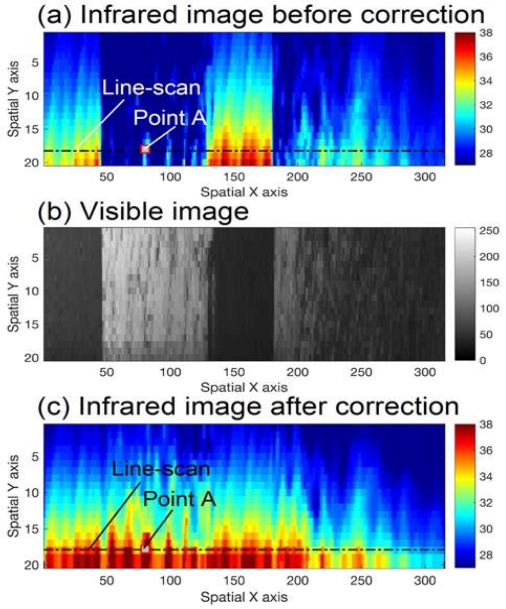

Fig 8. Emissivity correction of rail sample through the combination of two modality images, (a) infrared image before correction, (b) visible images and (c) infrared images after emissivity correction

The Fig. 9 illustrates a specific line-scanned infrared values and the transient thermal responses of point A as marked in Fig. 8. After correction, the line-scanned infrared values in the shiny area are enlarged close to the value of black paint conditions as shown in Fig. 9a. The higher infrared values contrast around cracks in shiny region shows the improved performance for defect detection. The transient thermal responses of point A in Fig. 9b demonstrate that the infrared values before correction are enlarged like that of black painted response in the heating stage. However, the correction results in the cooling stage as shown in Fig. 9b need more improvement by the optimization of the method, e.g. better selection of weight coefficient or additional correction factors. Compared to the infrared image of the black paint sample, the MSE calculation of the original infrared value in Fig. 9b with 2.58 and the recovered one with 0.33 validate the robust capability of the proposed method for emissivity correction.

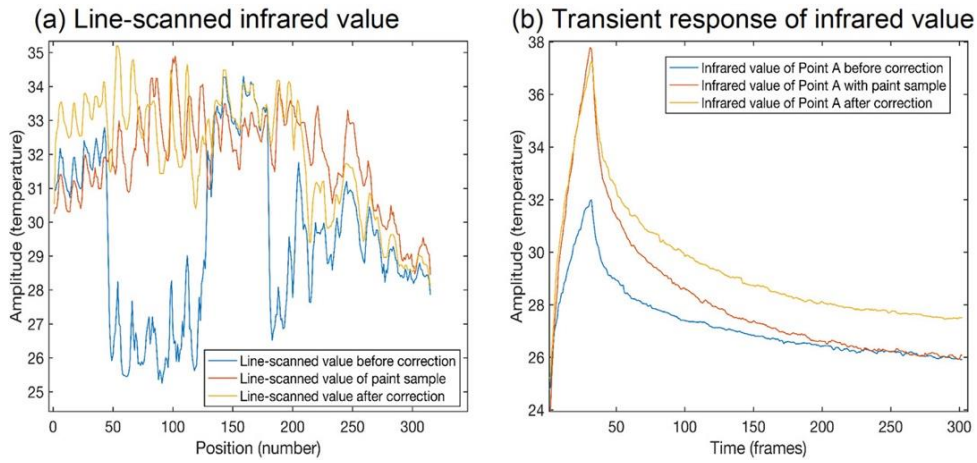

Fig. 9 Infrared images values comparison before and after emissivity correction, (a) specific line-scan infrared value and (b) transient thermal response with selected point A from figure 8.

In contrast to the transient thermal response of a specific point A in Fig. 9b, the infrared images of the rail sample before and after correction are illustrated in Fig. 10 considering the different heating and cooling times. The infrared images before correction shows significant emissivity variation influence on thermal patterns in the shiny and black paint areas. In the heating stage with frames 10 and 30, the infrared images after correction using the proposed method demonstrate the accurate mapping of thermal patterns for crack characterization. However, the different thermal pattern responses between the shiny and paint areas in the cooling stages e.g. frames 50 and 100 still need more improvement by the optimization of the method.

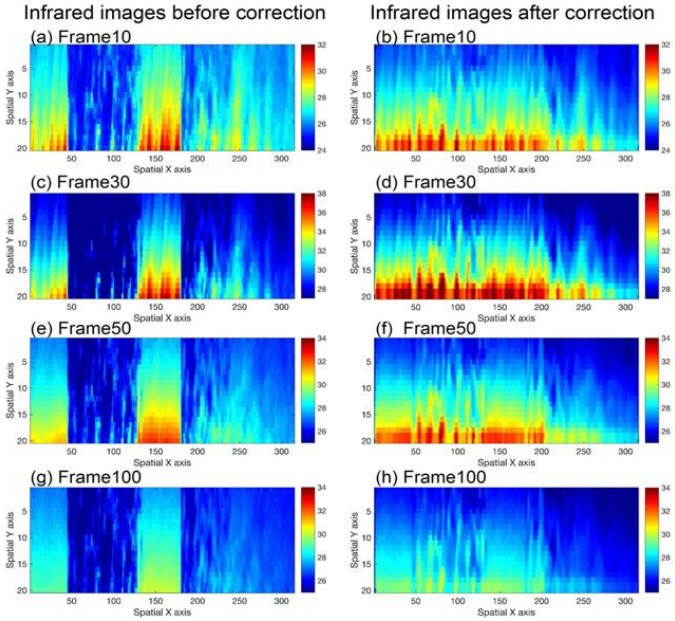

Fig 10. Emissivity correction results of infrared images Frame 10, 30, 50 and 100 at different heating and cooling times with demonstration (a, c, e, g) before correction and (b, d, f, h) after emissivity correction

4.3 Comparative analysis and discussion

To compare the proposed method with previous studies [4, 13], different infrared imaging results of the sample in Fig. 4c are illustrated in Fig. 11. The original infrared image before correction is shown in Fig. 11a. The infrared image after emissivity correction using the proposed method is shown in Fig. 11b. The normalized feature based on the Ref. [13] is shown in Fig. 11c. The Fig. 11d is the infrared image of Fig. 4b with full black paint. In contrast to Fig. 11a, all of the three correction results demonstrate more accurate results of thermal patterns for natural multiple cracks characterization as shown in Figs. 11b-11d. As discussed in references [13, 14], the normalization method eliminates the emissivity factor from the radiation equation (1) and uses the ratio or contrast results for defect

characterization. Several abnormal thermal contrast in local areas as shown in Fig. 11c demonstrate its limitation for quantitative evaluation. The infrared image with uniform black paint presents accurate thermal patterns without emissivity influence as shown in Fig. 11d. However, as we all know, it is difficult for the real application of thermography NDT because of the complex painting procedure and the pollution on test object. In contrast to the infrared image in Fig. 11d, the MSE calculation of the original image in Fig. 11a with 2.32 and the recovered image in Fig. 11b with 9.12 demonstrate the improved capability of the method to obtain accurate thermal patterns. Visually, Fig. 11b is most close to Fig. 11d. Above all, the propose method provides more advantages for emissivity correction and NDT applications: 1) it provides real thermal values and accurate infrared mapping of thermal patterns; 2) it does not need any complex painting procedure and with no pollution on test object; 3) it is independent on the surface emissivity variation influence and provides more information from both of the optical and infrared spectra by using two images.

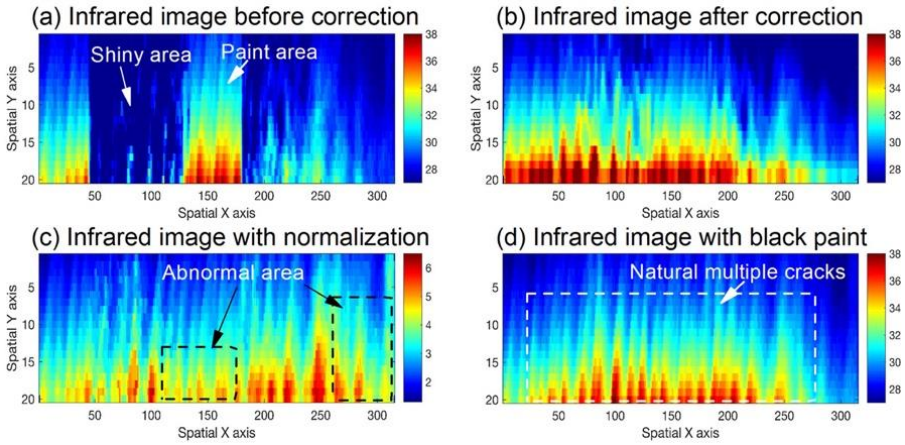

Figure 11. Comparison of emissivity correction results with (a) infrared image before correction, (b) correction by using two images, (c) normalization results and (d) infrared image with full black paint

5. Conclusion and future works

This paper proposes a new emissivity correction method by using two cameras measurement in different spectra. It has been applied for the optimized design of our developed ECPT system. A close spectrum correlation of infrared and visible images is identified to the monotonic relationship based on the physics behind the emissivity and reflectance. According to the retrieved spectrum correlation, the algorithms and invariant correction coefficient are developed to reduce the influence of the varying emissivity of an object in infrared thermography with respect to wavelength. It is used to correct the infrared values in shiny area for emissivity correction, which make it independent of emissivity. Experimental studies are performed for validation on a steel plate and rail samples with different known emissivity. The finding from the obtained results demonstrates the improved capability of the method for emissivity correction of infrared images. In contrast to previous methods, the proposed method presents much more advantages for further defect detection and quantitative NDE (QNDE) applications [4, 8].

Future works will be carried out to correct the infrared image with the unknown emissivity variation influences from different materials, surface roughness, coating layers e.g. with oil, water, oxidation on the top surface of metallic object [42, 43] with quantitative pseudo color different computation as measurement errors. The robustness evaluation of the proposed method will be conducted based on the providing information and results obtained with other different IR and visible cameras. The optimized ECPT system with two cameras will be developed for the 3D thermography by using the RGB-D device and for the QNDE [44] as well as the scanning inspection in high speed railway NDT applications [4, 8].

Acknowledgements

This work is funded by the National Natural Science Foundation of China (Grant No. 61527803 and 51377015) and the EPSRC IAA Phase 2: 3D super-fast and portable eddy current pulsed thermography (ECPT) (EP/K503885/1) for railway inspection project. The author would like to thank China Scholarship Council for sponsoring Mr. Yunlai Gao's visiting to Newcastle University, UK.

References

[1] Maldague, X. Applications of infrared thermography in nondestructive evaluation. Trends in optical nondestructive testing, 591-609, (2000).
[2] Shepard, S. M., Lhota, J. R., Rubadeux, B. A., Wang, D., & Ahmed, T. Reconstruction and enhancement of active thermographic image sequences. Optical Engineering, 42(5), 1337-1342, (2003).
[3] Holland, S. D., & Renshaw, J. Physics-based image enhancement for infrared thermography. NDT & E International, 43(5), 440-445, (2010).
[4] Gao, Y., Tian, G. Y., Wang, P., Wang, H., Gao, B., Woo, W. L., & Li, K. Electromagnetic pulsed thermography for natural cracks inspection. Scientific Reports, 7, (2017).
[5] Wang, Y., Gao, B., Tian, G., Woo, W. L., & Miao, Y. Diffusion and separation mechanism of transient electromagnetic and thermal fields. International Journal of Thermal Sciences, 102, 308-318, (2016).
[6] Gao, B., Yin, A., Tian, G., & Woo, W. L. Thermography spatial-transient-stage mathematical tensor construction and material property variation track. International Journal of Thermal Sciences, 85, 112-122, (2014).
[7] Avdelidis, N. P., & Almond, D. P. Transient thermography as a through skin imaging technique for aircraft assembly: modelling and experimental results. Infrared physics & technology, 45(2), 103-114, (2004).
[8] Netzelmann, U., Walle, G., Lugin, S., Ehlen, A., Bessert, S., & Valeske, B. Induction thermography: principle, applications and first steps towards standardisation. Quantitative InfraRed Thermography Journal, 13(2), 170-181, (2016).
[9] Tabatabaei, N., Mandelis, A., & Amaechi, B. T. Thermophotonic radar imaging: An emissivity-normalized modality with advantages over phase lock-in thermography. Applied Physics Letters, 98(16), 163706, (2011).
[10] Larciprete, M. C., Y. S. Gloy, R. Li Voti, G. Cesarini, G. Leahu, M. Bertolotti, and C. Sibilia. "Temperature dependent emissivity of different stainless steel textiles in the infrared range." International Journal of Thermal Sciences 113: 130-135, (2017).
[11] Ordonez-Miranda, J., & Alvarado-Gil, J. J. Infrared emissivity determination using a thermal-wave resonant cavity: comparison between the length- and frequency-scan approaches. International Journal of Thermal Sciences, 74, 208-213, (2013).
[12] Yuan, Z. Influence of non-ideal blackbody radiator emissivity and a method for its correction. International Journal of Thermophysics, 30(1), 220-226, (2009).
[13] Bai, L., Tian, S., Cheng, Y., Tian, G. Y., Chen, Y., & Chen, K. Reducing the effect of surface emissivity variation in eddy current pulsed thermography. IEEE Sensors Journal, 14(4), 1137-1142, (2014).
[14] Yang, R., He, Y., Gao, B., & Tian, G. Y. Inductive pulsed phase thermography for reducing or enlarging the effect of surface emissivity variation. Applied Physics Letters, 105(18), 184103, (2014).
[15] Ehlen, A; Netzelmann, U; Lugin, S; Finckbohner, M; Valeske, B; Bessert, S. Automated NDT of railway wheels using induction thermography, In 55th Annual British conference of NDT, (2016).
[16] Kasemann, M., Walter, B., Meinhardt, C., Ebser, J., Kwapil, W., & Warta, W. Emissivity-corrected power loss calibration for lock-in thermography measurements on silicon solar cells. Journal of Applied Physics, 103 (11), 113503, (2008).
[17] Vellvehi, M., Perpiñà, X., Lauro, G. L., Perillo, F., & Jordà, X. Irradiance-based emissivity correction in infrared thermography for electronic applications. Review of scientific instruments, 82(11), 114901, (2011).
[18] Schubert, M. C., Pingel, S., & Warta, W. Quantitative carrier lifetime images optically measured on rough silicon wafers. Journal of applied physics, 101(12), 124907, (2007).
[19] Maldague, X., Galmiche, F., & Ziadi, A. Advances in pulsed phase thermography. Infrared physics & technology, 43(3), 175-181, (2002).
[20] He, Y., Tian, G., Pan, M., & Chen, D. Eddy current pulsed phase thermography and feature extraction. Applied Physics Letters, 103(8), 084104, (2013).
[21] Gao, B., Bai, L., Woo, W. L., & Tian, G. Thermography pattern analysis and separation. Applied Physics Letters, 104(25), 251902, (2014).
[22] Schmugge, T., French, A., Ritchie, J. C., Rango, A., & Pelgrum, H. Temperature and emissivity separation from multispectral thermal infrared observations. Remote Sensing of Environment, 79(2), 189-198, (2002).
[23] Duvaut, T. Comparison between multiwavelength infrared and visible pyrometry: Application to metals. Infrared Physics & Technology, 51(4), 292-299, (2008).
[24] Madura, H., & Piatkowski, T. Emissivity compensation algorithms in double-band pyrometry. Infrared physics & technology, 46(1), 185-189, (2004).
[25] Hagqvist, P., Sikström, F., Christiansson, A. K., & Lennartson, B. Emissivity compensated spectral pyrometry - algorithm and sensitivity analysis. Measurement Science and Technology, 25(2), 025011, (2014).
[26] Netzelmann, U., & Abuhamad, M. Pulsed thermography in multiple infrared spectral bands. In Journal of Physics: Conference Series, 214(1): 012095. IOP Publishing. (2010).
[27] Xing, J., Cui, S., Qi, W., Zhang, F., Sun, X., & Sun, W. A data processing algorithm for multi-wavelength pyrometry - which does not need to assume the emissivity model in advance. Measurement, 67, 92-98, (2015).
[28] Mendenhall, M. J., Nunez, A. S., & Martin, R. K. Human skin detection in the visible and near infrared. Applied Optics, 54(35), 10559-10570, (2015).
[29] Momeni, M., & Saradjian, M. R. Evaluating NDVI-based emissivities of MODIS bands 31 and 32 using emissivities derived by Day/Night LST algorithm. Remote Sensing of Environment, 106(2), 190-198, (2007).
[30] Tachikawa, Y., Sugimoto, J., Takada, M., Kawabata, T., Lyth, S. M., Shiratori, Y., & Sasaki, K. In Operando Visualization of SOFC Electrodes by Thermography and Visible Light Imaging. ECS Electrochemistry Letters, 4(11), F61-F64, (2015).
[31] Echániz, T., Pérez-Sáez, R. B., & Tello, M. J. Optical properties of metals: Infrared emissivity in the anomalous skin effect spectral region. Journal of Applied Physics, 116(9), 093508, (2014).
[32] Herve, P., Cedelle, J., & Negreanu, I. Infrared technique for simultaneous determination of temperature and emissivity. Infrared Physics & Technology, 55(1), 1-10, (2012).
[33] Haiyan Jin, Yanyan Wang, A fusion method for visible and infrared images based on contrast pyramid with teaching learning based optimization, Infrared Physics & Technology, Volume 64, Pages 134-142, (2014).
[34] Tian, G. Y., Gledhill, D., Taylor, D., & Clarke, D. Colour correction for panoramic imaging. In Information Visualisation, Proceedings. Sixth

International Conference on (pp. 483-488). IEEE. 2002.
[35] Finlayson, G. D., & Tian, G. Y. (1999). Color normalization for color object recognition. International Journal of Pattern Recognition and Artificial Intelligence, 13(08), 1271-1285.
[36] Gao, Y., Tian, G.Y., Wang, P., Wang, H., Emissivity correction of eddy current pulsed thermography for rail inspection. In Proceedings of 2016 IEEE Far East NDT New Technology & Application Forum (FENDT), pp. 108-112, IEEE, 2016.
[37] Tang, C., Tian, G.Y., Chen, X., Wu, J., Li, K., Meng, H., Infrared and visible images registration with adaptable local-global feature integration for rail inspection. Infrared Physics & Technology, 87, 31-39, 2017.
[38] Fan, M., Cao, B., Tian, G., Ye, B., & Li, W. (2016). Thickness measurement using liftoff point of intersection in pulsed eddy current responses for elimination of liftoff effect. Sensors and Actuators A: Physical, 251, 66-74.
[39] Fan, M., Huang, P., Ye, B., Hou, D., Zhang, G., & Zhou, Z. (2009). Analytical modeling for transient probe response in pulsed eddy current testing. NDT & E International, 42(5), 376-383.
[40] Gao, Y., Tian, G. Y., Li, K., Ji, J., Wang, P., & Wang, H. Multiple cracks detection and visualization using magnetic flux leakage and eddy current pulsed thermography. Sensors and Actuators A: Physical, 234, 269-281, (2015).
[41] Tian, G. Y., Gao, Y., Li, K., Wang, Y., Gao, B., & He, Y. Eddy current pulsed thermography with different excitation configurations for metallic material and defect characterization. Sensors, 16(6), 843, (2016).
[42] Shi, D., Liu, Q., Zhu, Z., Sun, J., & Wang, B. (2014). Experimental study of the relationships between the spectral emissivity of brass and the temperature in the oxidizing environment. Infrared Physics & Technology, 64, 119-124.
[43] Holland, S. D. Thermographic signal reconstruction for vibrothermography. Infrared Physics & Technology, 54(6), 503-511, (2011).
[44] Marinetti, S., & Cesaratto, P. G. Emissivity estimation for accurate quantitative thermography. NDT & E International, 51, 127-134, (2012).

Biographies

Yunlai Gao received the B.Sc. degree in the School of Automation and Electrical Engineering from Zhejiang University of Science and Technology, Hangzhou, China, in 2010, and the M.Sc. degree in College of Automation Engineering from Nanjing University of Aeronautics and Astronautics, Nanjing, China, in 2013. He is currently working toward the Ph.D. degree in electromagnetic and thermography non-destructive evaluation (NDE) in the Nanjing University of Aeronautics and Astronautics (NUAA), Nanjing, China. His research interests include novel sensor design, electromagnetic and thermography NDE, signal processing.

Gui Yun Tian received the B.Sc. degree in metrology and instrumentation and M.Sc. degree in precision engineering from the University of Sichuan, Chengdu, China, in 1985 and 1988, respectively, and the Ph.D. degree from the University of Derby, Derby, U.K., in 1998. From 2000 to 2006, he was a Lecturer, Senior Lecturer, Reader, Professor, and Head of the group of Systems Engineering, respectively, with the University of Huddersfield, U.K. Since 2007, he has been based at Newcastle University, Newcastle upon Tyne, U.K., where he has been Chair Professor in Sensor Technologies. Currently, He is also an adjunct professor in the College of Automation Engineering, Nanjing University of Aeronautics and Astronautics. He has coordinated several research projects from the Engineering and Physical Sciences Research Council (EPSRC), Royal Academy of Engineering and FP7, on top of this he also has good collaboration with leading industrial companies such as Airbus, Rolls Royce, BP, nPower and TWI among others.